Journal of Power Sources 207 (2012) 134–140

Contents lists available at SciVerse ScienceDirect

Journal of Power Sources

journal homepage: www.elsevier.com/locate/jpowsour

Correlation between dissolution behavior and electrochemical cycling performance for $LiNi_{1/3}Co_{1/3}Mn_{1/3}O_2$-based cells

Honghe Zheng[a,b,*], Qingna Sun[a], Gao Liu[b], Xiangyun Song[b], Vincent S. Battaglia[b]

[a] School of Energy, Soochow University, Suzhou, Jiangsu 215006, PR China
[b] Lawrence Berkeley National Laboratory, 1 Cyclotron Rd, Berkeley, CA 94720, USA

ARTICLE INFO

Article history:
Received 10 November 2011
Received in revised form 19 January 2012
Accepted 21 January 2012
Available online 8 February 2012

Keywords:
Lithium ion batteries
Cathode
Charge voltage limit
Cycling performance
Battery failure mechanism

ABSTRACT

$LiNi_{1/3}Co_{1/3}Mn_{1/3}O_2$ (NCM) cathode has wide operation voltage window. Dissolution behavior of the NCM cathode at different charge states in 1 M $LiPF_6$/EC:DEC (1:1) electrolyte is determined with inductively coupled plasma (ICP) technique. Electrochemical cycling performance of the NCM-based cells in the electrolyte with different charge voltage limits is correlated with the dissolution of the active material. With increasing charge voltage limit, specific capacity and energy density of the electrode are significantly enhanced. However, cycle life of the cell based on NCM cathode and meso-carbon micro-bead (MCMB) anode is compromised at cutoff voltages >4.3 V. Mechanisms of the capacity decay for the full cell cycled with high charge voltage limit are investigated. Impedance rise of the graphite anode, which is resulted from deposition of the dissolved metal ions from the NCM cathode, is specified to be the main factor responsible for the cell failure. SEM observation and EDX analysis confirm the presence of Mn, Co, and Ni elements on the MCMB anode surface when the cell is cycled with high charge voltage limits.

1. Introduction

A worldwide effort to develop electric vehicles (EVs) to dramatically reduce the consumption of petroleum fuels in the transportation sector is in full swing [1–4]. Nowadays, the key technological barriers that hinder the commercial adoption of lithium-ion batteries for plug-in hybrid-electric-vehicles (PHEVs) are their low energy density, high cost and limited calendar and cycle life. $LiNi_{1/3}Co_{1/3}Mn_{1/3}O_2$ (NCM) cathode material demonstrates high capacity, milder thermal instability in the charged state, lower cost, and less toxicity. In addition, this material undergoes a small volume change of about 3% during Li insertion and extraction, proving to be beneficial with regard to cycling stability, cell life, and rate capability. For this promising cathode of lithium ion batteries for PHEV applications, much attention is given to the development of reliable synthetic routes and its structural analysis and basic electrochemical behavior. Studies on the structural analysis are reaching a very high level of precision by using different modern spectroscopic techniques [5–7]. However, long-term cycling behavior of this material and the capacity fading mechanisms of the full cell under different cycling conditions remain a significant problem.

Unlike other commonly used cathode materials in lithium-ion batteries such as $LiCoO_2$ and $LiFePO_4$, which operate on flat voltage plateaus, NCM cathode can be operated with very different charge voltage limits since the phase-transition is suppressed owing to Mn^{4+} in the lattice. Almost linear increase of specific capacity can be obtained with increase of charge voltage from 4.2 to 4.7 V *vs.* Li/Li^+, and even higher potentials [8,9]. As a result, the electrochemistry reaction is endlessly impelled to complete, and capacity is increased as more Li^+ is reversibly de-inserted and inserted. As cell energy is proportional to the capacity times the voltage, operation of the cell with higher charge voltage contributes to a quadratic increase in energy density. Meanwhile, remove of more Li^+ induces the oxidation of more Ni^{2+} and Co^{2+}. Long-term cycling behavior of the cell may be worsened due to the increased dissolution of the active material into the electrolyte and the possible electrolyte oxidation at the electrode/electrolyte interface. Therefore, an optimum charge voltage limit is important for the NCM-based cell to obtain high energy output without reducing its cycle life. It will also be of a good help for developing adequate testing protocols and design appropriate testing procedures. However, to the best of our knowledge, the optimum operation voltage for this material to demonstrate both high capacity and long cycle-life has not been explained.

In this work, dissolution of the NCM cathode at different charge states in 1 M $LiPF_6$/EC:DEC (1:1) electrolyte was determined. The capacity, energy and long-term cycling properties of the NCM-based cells at different charge voltage limits were investigated.

* Corresponding author at: Soochow University, School of Energy, 1 Shizi St, Suzhou, Jiangsu 215006, PR China. Tel.: +86 512 69153523; fax: +86 512 67870271.
E-mail address: hhzheng66@yahoo.com.cn (H. Zheng).

0378-7753/$ – see front matter © 2012 Elsevier B.V. All rights reserved.
doi:10.1016/j.jpowsour.2012.01.122

From these, we discussed the correlation between the dissolution of the cathode material and the long-term cycling behavior of the full cell based on NCM cathode and meso-carbon micro-bead (MCMB) anode. An optimum charge voltage limit for the cathode having high energy output and long cycle life is obtained. The results are informative in developing an understanding of the charge–discharge mechanism in this system.

2. Experimental

NCM cathode laminates were manufactured by Seimi based on specifications provided by Argonne National Laboratory. The cathode composition is 80 (wt)% NCM, 10 (wt)% poly(vinylidene difluoride) (PVDF) binder, and 10 (wt)% acetylene black. The laminate is about 57 μm thick at 30% porosity casting on 22 μm thick Al foil with an active material loading of about 13.3 mg cm^{-2}. The anode material adopted in this study is meso-carbon micro-beads (MCMB10-28) obtained from Osaka Gas. The anode consists of 85.6 (wt)% MCMB10-28, 8 (wt)% PVDF binder, and 6.4 (wt)% acetylene black. The laminate is 64 μm thick at 35% porosity casting on 18 μm thick copper foil with an active material loading of about 8.0 mg cm^{-2}. There is always an excess capacity for the anode compared with the cathode. An electrolyte of 1 M $LiPF_6$ in EC/DEC 1:1 (weight ratio) electrolyte from Ferro was used in this study.

Dissolution of metal ions from the NCM cathode into the electrolyte was determined by inductively coupled plasma (ICP) technique. After charging to the different voltages in a sealed beaker cell, the electrode was taken out and thoroughly washed with pure DMC solvent. After drying under vacuum at room temperature, 0.2 g of the electrode laminate removed from the Al substrate was added into a vial containing 15 g of 1 M $LiPF_6$/EC:DEC (1:1) electrolyte. The bottle was rotated at 20 rpm at room temperature for 4 weeks. After allowing the mixture to settle overnight, 1 ml of the electrolyte was taken out and mixed with 10 g HNO_3 in order to completely digest the organic solvent. Once the mixture equilibrated enough, de-ionized water was added to make 50 ml of the solution. Calibration standards were made from Merck standard solutions and were formulated to be matrix matched to the obsidian samples. The working curve was obtained with a blank and four standard samples containing 0.01 ppm, 0.1 ppm, 1 ppm, and 10 ppm of Ni^{2+}, Co^{2+}, and Mn^{2+}, respectively. Following the ICP protocol, the dissolved amounts of Mn, Co, and Ni elements in the electrolyte were determined.

Half-cells and full-cells were fabricated with standard 2325 coin cell hardware, as described in Ref. [10]. The NCM cathode electrode area was 1.26 cm^2 and the MCMB anode area was 1.60 cm^2. For the half-cells, the charge voltage limit was varied from 4.2 to 4.7 V *vs.* Li/Li^+. Considering the working plateau for MCMB is *ca.* 0.1 V *vs.* Li/Li^+, the upper voltage limit for the full-cells was varied from 4.1 to 4.6 V. All lower cut-off voltages were set at 3.0 V. Electrochemical tests were carried out using a Maccor Battery Cycler in a Thermotron Environmental Chamber set at 303 K. Ten formation cycles were performed at *C*/10 for half cells and at *C*/24 for full cells. The last discharge capacity of the formation cycles was used to estimate the reversible capacity of the cells and used for estimating the 1*C*-rate on discharge for subsequent cycling. Long-term cycling test of the full-cells was carried out by *C*/2 charge to a predefined upper voltage limit and held at this voltage until the current dropped to *C*/10, and then discharged at 1*C* until the cell voltage reached 3.0 V. Each cell was cycled 500 times.

Upon completion of the long-term cycling, the cell was charged to a potential of 4.0 V and held at the voltage under 30 °C for 5 h. The impedance spectra (100 kHz to 10 mHz, 5 mV perturbation) of the cells were recorded using a Solartron 1286. Afterwards, the coin cells were dissembled in a glove box in their fully discharged state. Both anode and cathode were harvested and assembled into new half-cells to evaluate their electrochemical performance. For the harvested NCM cathode, the new half cells were charged at *C*/10 to 4.5 V and then discharged at rates of *C*/10, *C*/5, *C*/2, 1*C*, 2*C*, 5*C*, and 10*C*, respectively. The same procedure was applied on the harvested MCMB anode. The new half cells containing the harvested MCMB anode were cycled between 0.01 and 1 V at different rates.

After being fully discharged, the harvested electrodes were taken out from all the half cells, washed for 3 times with DMC solvent, and dried under vacuum for 2 h. Crystal structure of the NCM cathode before and after long-term cycling test with different charge voltage limits was characterized with an automated Rigaku X-ray diffractometer using a Cu K(α) radiation (λ = 1.5405 Å). The diffraction angle (2θ) was measured between 15° and 70° with an increment of 1° min^{-1}. SEM imaging of the harvested electrode was performed with a JEOL JSM-7500F SEM. This equipment is also capable of energy dispersive X-ray spectroscopy (EDX), which is used to detect foreign elements deposited on the MCMB anode surface after cycling. The determination error is estimated to be within 30%.

3. Results and discussion

Fig. 1 shows the first charge and discharge profiles of the NCM half-cell cycled with different charge voltage limits at *C*/10 rate. As seen in this figure, an increase of charge capacity is obtained by increasing the charge voltage limit from 4.2 to 4.7 V. Correspondingly, the discharge curve is sloped with a nearly linear increase of the specific capacity from 4.0 to 4.7 V. Ohzuku's group and Chang's group proposed that the Ni^{2+}/Ni^{4+} couple occurs at 3.7–4.0 V and the oxidation of Co^{3+} to Co^{4+} follows above 4.5 V [11,12]. As the result, the specific capacity is increased from 134.4 up to 198.1 mAh g^{-1} by elevation of the charge voltage limit from 4.2 to 4.7 V. This corresponds to an almost 10% capacity rise per 0.1 V of voltage rise. Table 1 provides a summary of the cell discharge capacity, cell energy, and average cell voltage on discharge for the NCM cathode cycled with different charge voltage limits. The average cell voltage is defined as the ratio of energy density *vs.* the specific capacity. As seen in the table, a total increase of 53.5% of energy density is obtained by pushing the charge voltage limit from 4.2 to 4.7 V.

Fig. 2 displays the first coulombic efficiency and the discharge capacity of the NCM cathode at the first and the tenth cycles as a function of charge voltage limit obtained from the initial 10 formation cycles. This cathode has low coulombic efficiency (less than 90%) at the first cycle, indicating the existence of irreversible

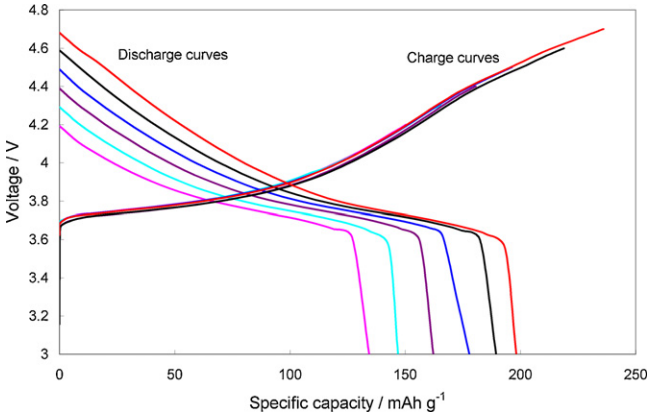

Fig. 1. The first charge and discharge curves of the NCM half cell operated with different upper voltage limits at *C*/10.

Table 1
Discharge capacity, energy density and average cell voltage for the NCM-based half cell cycled with different charge voltage limits.

Charge voltage (V *vs.* Li/Li$^+$)	Discharge capacity (mAh g^{-1})	Energy density (mWh g^{-1})	Average cell voltage (V)
[4.2]	134.4	513.4	3.82
[4.3]	146.8	566.6	3.86
[4.4]	162.1	630.6	3.89
[4.5]	177.8	697.0	3.92
[4.6]	189.4	748.1	3.95
[4.7]	198.1	788.4	3.98

intercalation sites and irreversible phase transformation at the first cycle. A maximum coulombic efficiency of 88.7% at the first cycle is obtained with 4.4 V charge voltage. So far, several factors have been proposed explaining the high irreversible capacity of NCM cathode. The first one occurred at the early stage of charge is the mixing of Li and Ni within the lattice. Li-sites occupied by Ni can reduce the vacant site available for lithium. The second one is associated with the oxidation reaction of electrolyte at the electrode/electrolyte interface. In addition, oxygen release from NCM at high electrode potential can also lead to an irreversible capacity loss in the first cycle. Considering the irreversible capacity relating to the irreversible intercalation sites at the first cycle is consumed at the earlier stage of the charge and some of the reversible lithium is not available at lower potentials, reducing charge voltage leads to lower first coulombic efficiency. When the cell voltage exceeds 4.5 V, other kinds of irreversible reaction, *i.e.* electrolyte oxidation and oxygen release, are triggered. The first coulombic efficiency begins to decrease with increasing charge voltage as the electrolyte oxidation and oxygen release from the cathode are intensified by elevation of the electrode potentials. Discharge capacity of the cathode with electrochemical cycles is also affected by the charge voltage limit. Although there is a monotonous increase of discharge capacity at the first cycle with increasing charge voltage, after 10 cycles, a considerable capacity loss is observed when the charge voltage exceeds 4.6 V.

Among different reasons for capacity fade of Li-ion battery cathodes, dissolution of active material is always considered to be the primary one [13]. Operating voltage is one of the important factors determining the dissolution rate of metal ions. Fig. 3 shows the concentrations of Mn, Co, and Ni cations found in the electrolyte for the electrode at different potentials under room temperature for 4 weeks. It is seen that high charge state accelerates the loss of metal elements from the NCM cathode into the electrolyte. The concentration of Mn cations is considerably higher than that of Co and Ni cations at each charge state, implying that Mn is easier to

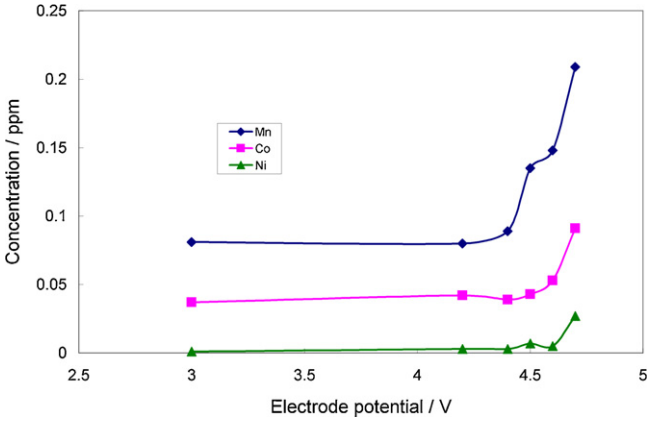

Fig. 3. Concentrations of Mn, Co and Ni elements in 1 M $LiPF_6$/EC + DEC (1:1) electrolyte when the cathode is polarized to different potentials.

be removed from the NCM electrode and dissolve into the electrolyte than Co and Ni elements. Dissolution of Ni is only observed when the electrode potential is higher than 4.6 V *vs.* Li/Li$^+$. Overall, a dramatic increase of the dissolved Mn, Co, and Ni elements in the electrolyte is seen at potentials higher than 4.5–4.6 V.

So far, two different mechanisms of manganese dissolution are proposed. One is manganese disproportional reaction according to $2Mn(III) \rightarrow Mn(IV) + Mn(II)$ (solv) route [14,15]. The other one is ascribed to acid corrosion catalyzed by HF and other organic acids according to the following scheme [16,17]:

$$Li_{1-x}Mn_2O_4 + 2(1-x)HF \rightarrow ((3+x)/4)\lambda\text{-}Mn_2O_4 + (1-x)LiF + (1-x)H_2O + ((1-x)/2)MnF_2$$

Considering there is trace Mn(III) in the NCM cathode aroused from defects or oxygen vacancy, the dissolved Mn may be associated with the disproportional reaction of Mn(III) at lower electrode potentials. However, at potentials higher than 4.5 V, where all the Mn(III) is oxidized to Mn(IV), the main source of the dissolved Mn is believed to come from acid corrosion. This process is catalyzed by acid species produced at high potentials due to the electrolyte oxidation at the electrode/electrolyte interface. The dramatic increase of metal ions is in agreement with the severe capacity fade of the cathode cycled with charge voltage limit higher than 4.6 V as shown in Fig. 2.

To examine the impact of charge voltage limit on the long-term cycling performance of the NCM-based full cell, MCMB-NCM full cells were fabricated and tested with different upper voltage limits. The first discharge curves of the MCMB-NCM full-cells charged

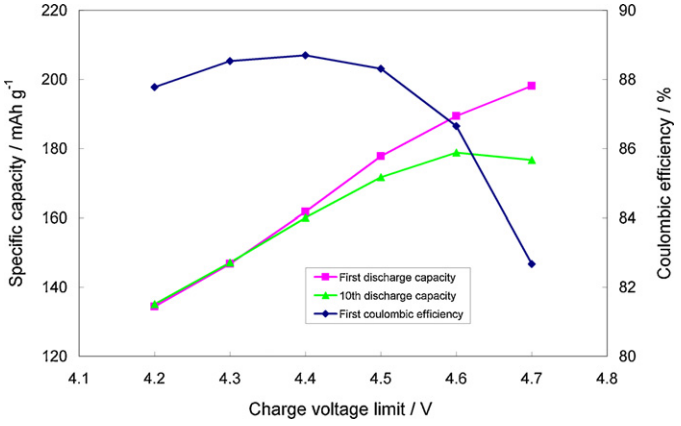

Fig. 2. The first coulombic efficiency and the discharge capacity of the NCM cathode at the first and the tenth cycles as a function of the charge voltage limit.

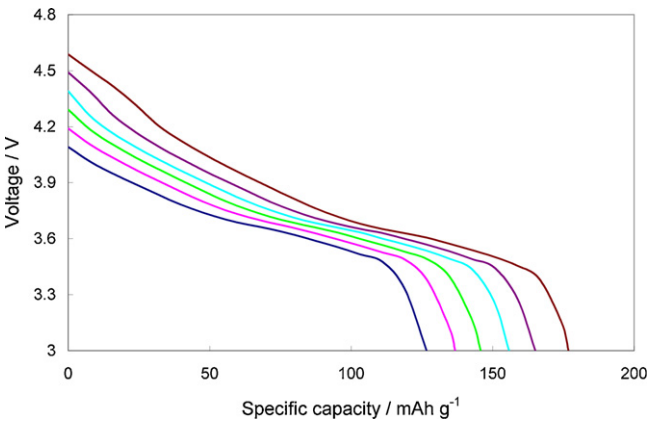

Fig. 4. The first discharge curves of the MCMB-NCM full cell formed with different charge voltage limits at *C*/24.

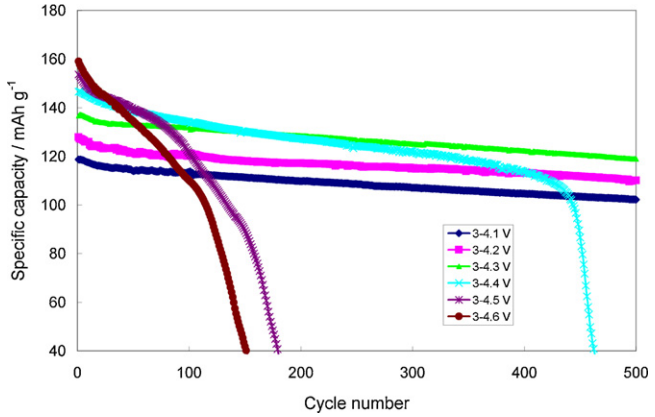

Fig. 5. Deep cycling performances of the MCMB-NCM full cell cycled with different charge voltage limits (*C*/2 charge and 1*C* discharge).

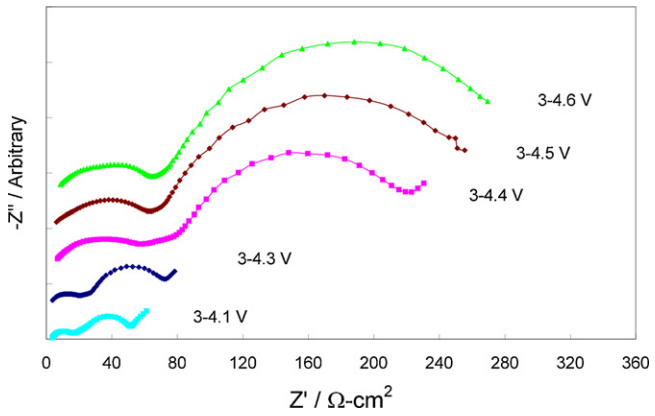

Fig. 6. Nyquist plots of the MCMB-NCM full cells after long-term cycling test with different charge voltage limits at 4.0 V.

to different charge voltage limits are displayed in Fig. 4. With increasing charge voltage limit, specific capacity of the NCM cathode increased from 126.7 to 177.3 mAh g^{-1}. Correspondingly, the energy density was increased from 466.7 to 677.9 mWh g^{-1}. A 40% capacity increase and a 45% energy increase were obtained by pushing the charge voltage from 4.1 to 4.6 V. In other words, about 8% capacity increase and 9% energy increase was achieved per 0.1 V increase of charge voltage.

In order to achieve high energy density of the cell without reducing its cycle life, it is required to charge the cell to an optimum charge voltage limit during electrochemical cycles. With this in mind, full cycling of the cell to different charge voltage limits was performed, the results of which are provided in Fig. 5. It is clear that the charge voltage limit significantly affected both the capacity and the cycle life of the cells. Although there is a significant capacity increase in the initial cycles by increasing charge voltage, cycle life of the cell is compromised when the charge voltage exceeds 4.3 V. After 500 cycles, the cells cycled between 3 and 4.1 V and 3 and 4.3 V showed less than 10% capacity decline. The fade-rate is steady and very similar for these two cells. This result compares favorably to that reported in literature in which more than 40% capacity was lost after 300 cycles between 2.75 and 4.2 V [6,18]. Hence, the NCM-based full-cells cycled are capable of much longer cycle life than previously reported. When cycled between 3 and 4.4 V, a slow fading rate was observed in the first 400 cycles, after which the cell capacity depleted quickly. The cells cycled between 3 and 4.5 V and 3 and 4.6 V demonstrated less than 150 cycles. A steep decline of capacity occurs after 80 cycles for the 4.5 V upper voltage limit cell and from the beginning for the 4.6 V upper voltage limit cell. From the cycling results, a charge voltage limit of 4.3 V is considered optimum for the cell having both high capacity and long cycle life.

Capacity fade of Li-ion batteries is associated with a number of processes and their interactions, including electrochemical, chemical, and even mechanical degradations, in both cathodes and anodes. Impedance rise is always one of the immediate results of these processes and interactions [19]. After long-term cycling test, EIS data for the cells cycled with different charge voltage limits were obtained at a cell voltage of 4.0 V as shown in Fig. 6. Both the high-frequency semi-circle and the following the mid-low frequency semicircle grew with increasing charge voltage limit. When the charge voltage limit exceeds 4.4 V, the cell exhibits very high impedance. It means that high charge voltage limit caused a dramatic impedance increase of the cell during electrochemical cycles. The resulting high cell impedance makes it difficult for Li migration between cathode and anode at the cycling rate. In this sense, it is possible to maintain low cell impedance for longer cycle life simply by optimizing the charge voltage limit for the cell based on NCM cathode and graphite anode.

In order to identify the impedance rise mechanism of the MCMB/NCM couple operated at high charge voltage limits, the full cells, after long term cycling to either negligible capacity or 500 cycles, were opened and subjected to post mortem analysis. Fig. 7 shows the XRD patterns of the pristine NCM electrode and after long term cycling to different charge voltage limits. The clear splitting of the reflections assigned to the Miller indices (0 0 6, 1 0 2) and (1 0 8, 1 1 0) for the pristine cathode indicates a well-layered structure. After long-term cycling with increasing charge voltage limit, the typical 0 0 3 peaks slightly shift to lower angles whereas the 1 0 1 and the 1 1 0 peaks shift to higher angles, indicating the lattice shrinkage along *a*, *b* direction and expansion along *c* direction [5,20,21]. The shift of 0 0 3 peaks for the 4.1 V and 4.3 V samples is larger than that of the 4.6 V sample. This is because the 4.1 V and 4.3 V samples underwent 500 cycles while 4.6 V sample lasted no more than 200 cycles in the cycling test. It reveals that the lattice shrinkage along *a*, *b* direction and expansion along *c* direction is associated with the cycle number and the depth of Li insertion and extraction during each cycle. Compared with Fig. 5, the change of the structural parameters has no much effect on the electrochemical behavior of the NCM cathode. As it is believed, the disappearance of 0 0 6 peak should be associated with the mixing of Li with the transition metal ions [12,22,23]. Despite with these small structural changes, XRD pattern of the harvested cathode, even cycled with 4.6 V charge voltage that suffered from severe metal ion dissolution

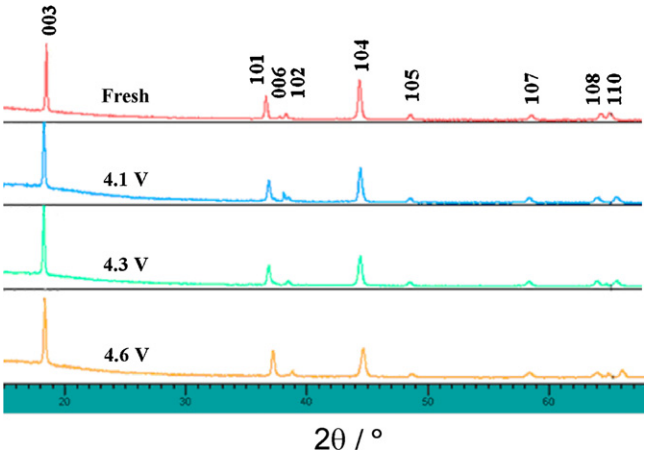

Fig. 7. XRD patterns of the fresh and harvested NCM electrodes cycled against MCMB anode with different charge voltage limits.

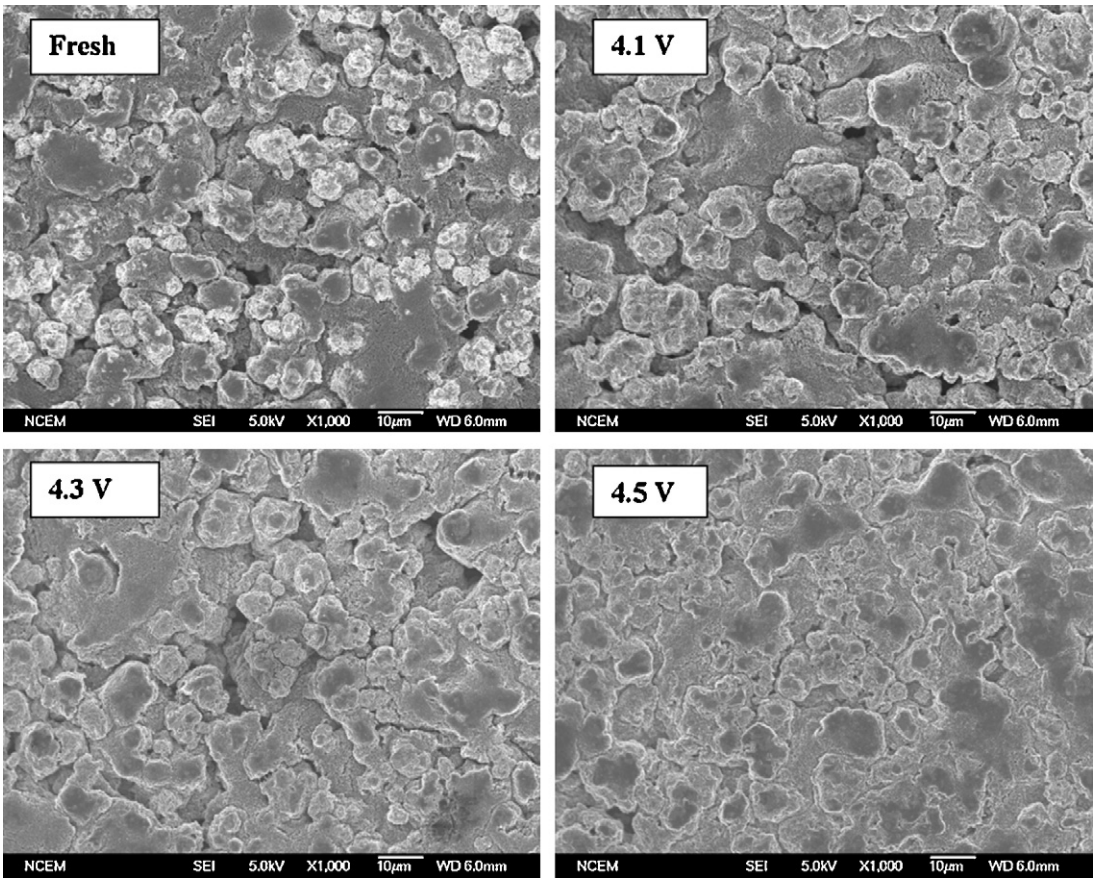

Fig. 8. SEM images of the fresh and harvested NCM cathodes cycled against MCMB anode with different charge voltage limits.

and capacity fade, did not show much structural differences as compared to that survived 500 cycles with lower charge voltage limit. This means that structural change of NCM is not a major contributor to the capacity fade. The conclusion is consistent with the literature reported by Li et al. [24], in which they showed that the delithiated NCM exhibited good crystal structural stability.

Morphologies of the fresh and the harvested NCM cathodes cycled with different upper voltage against MCMB anode are displayed in Fig. 8. With increasing charge voltage limit, the NCM particle size is increased and the electrode appears to be less porous. The particle size increase should be aroused from the deposition of a coating layer on the active material particles. Formation of the coating layer is associated with the electrolyte oxidation during prolonged electrochemical cycles. Oxidation reactions of the electrolyte components at the electrode/electrolyte interface are accelerated by elevation of the cell voltage. The resulted carbon-based substances precipitated on the active material particles and filled in the open space of the cathode. The layer is poor in conductivity and may hinder Li ion migration during electrochemical processes [25].

Electrochemical properties of the NCM cathode before and after long term cycling were also examined. Fig. 9 shows the rate performance of the fresh and harvested cathodes. Compared with the fresh electrode, about 15% and 23% capacity loss is observed at 0.1*C* for the harvested NCM cathode cycled against MCMB anode with 4.5 and 4.6 V charge voltage, respectively. As discussed above, the most important source of the capacity fade is aroused from the loss of the active material through dissolution. Of course, other factors such as phase transition of the electrode undetectable by XRD cannot be denied. Rate capability of the harvested NCM cathode is shown worse than that of the fresh electrode. This should be associated with the impedance rise aroused from the deposition of carbon-based substances onto the electrode as seen in Fig. 8. However, even at 1*C* rate (the cycling rate of the full cells), 22% and 30% capacity loss for the 4.5 V and 4.6 V cycled NCM cathode does not account for the almost 100% capacity loss of the full cell, for the cathode still delivers more than 70% of its capacity. It means the capacity loss and impedance rise at the cathode are not the most important source for the failure of the full cell operated with high charge voltage.

SEM images of the pristine and harvested MCMB electrode cycled against NCM with 4.3 and 4.5 V charge voltage limits are provided in Fig. 10. Compared with the pristine electrode, there is

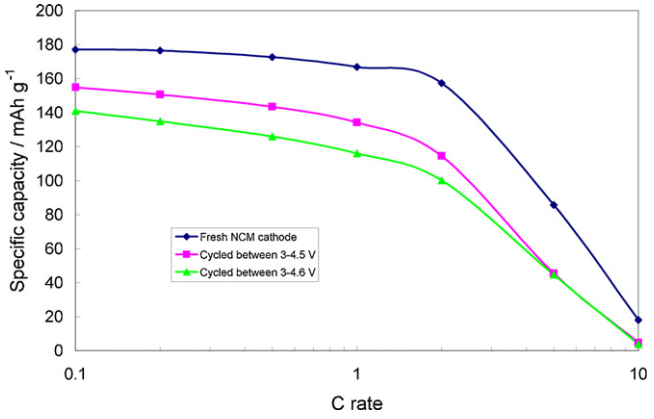

Fig. 9. Rate performance of the fresh and harvested NCM cathodes cycled against MCMB anode with 4.5 V and 4.6 V charge voltage limits.

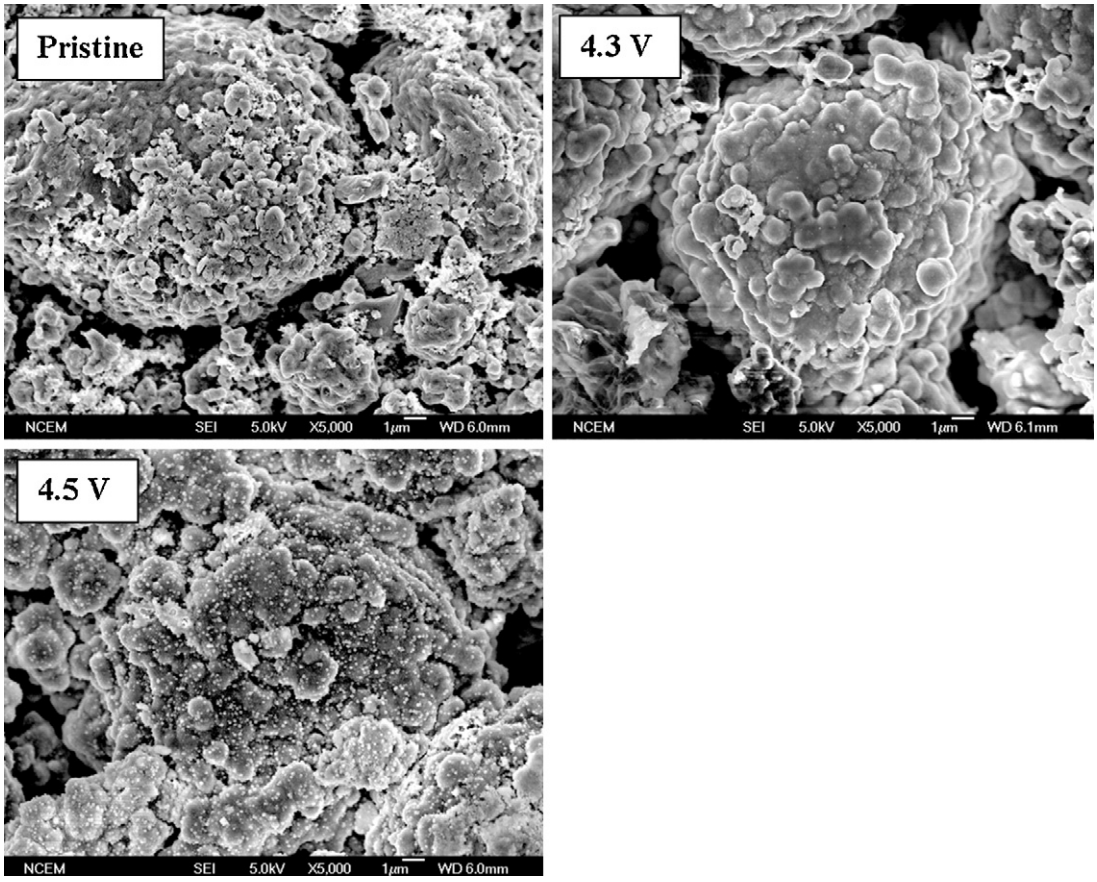

Fig. 10. SEM images of the fresh and harvested MCMB anodes cycled against NCM cathode with 4.3 V and 4.5 V upper voltage limits.

a very thick coating layer on the surface of the harvested MCMB cycled with 4.3 V charge voltage limit, which is believed to be associated with the accumulation of SEI components during repeatedly electrochemical cycles. Besides this, many small particles were seen on the surface of the harvested MCMB cycled with 4.5 V charge voltage limit. The possible source of the small particles dispersed on the MCMB surface could be the dissolved active material from the cathode during the electrochemical cycling. The dissolved transition metal ions migrate to the anode through the separator and deposit on the graphite surface as inorganic salts [26,27].

In order to get more information about the small particles, a specified small part with a white particle on the MCMB anode was subject to EDX analysis. Fig. 11 shows the result of the elemental analysis carried out by EDX using an X-ray detector attached to the SEM instrument. C, O, F, and P are the main elements detected. O is attributed to the solid electrolyte interface (SEI) components of different Li salts and F is attributed to the PVDF binder and some SEI components. P may also exist in the SEI components on the carbon surface. Besides these main elements, Mn, Ni, Co, and even Al elements were detected. Clearly, these elements are coming from the cathode. During prolonged electrochemical cycles at high operating voltages, Mn, Co, and Ni have found their way into the electrolyte as soluble species [27–30]. Of course, corrosion of Al is also possible when the cell is polarized to a high voltage limit [31,32].

To see the impact of the precipitation of the transition metal elements on the electrochemical performance of the anode, a comparison of rate performance between the fresh and harvested MCMB anodes cycled with 4.5 and 4.6 V charge voltage is provided in Fig. 12. The harvested MCMB anodes are seen having considerably high impedance as it is evident from their very poor rate performance. At 1C, the same rate as the full cell cycling condition, the anode lost about 80% of its capacity. Considering that the harvested cathode retained more than 70% of its initial capacity at the same rate, the failure of the full cell is more likely to be due to the deterioration of the anode. This result shows that the electrochemical performance of the graphite anode is profoundly influenced by the dissolved transition metal ion contaminants in the electrolyte solutions [33,34].

Dissolution behavior of the NCM cathode at different charge states shown in Fig. 3 can help to understand the long-term cycling

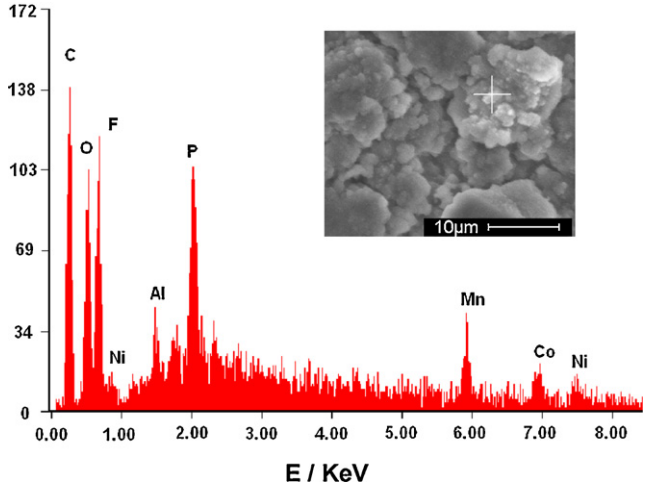

Fig. 11. EDX result of the harvested MCMB anode cycled against NCM cathode with 4.5 V voltage limit taken from the designated area.

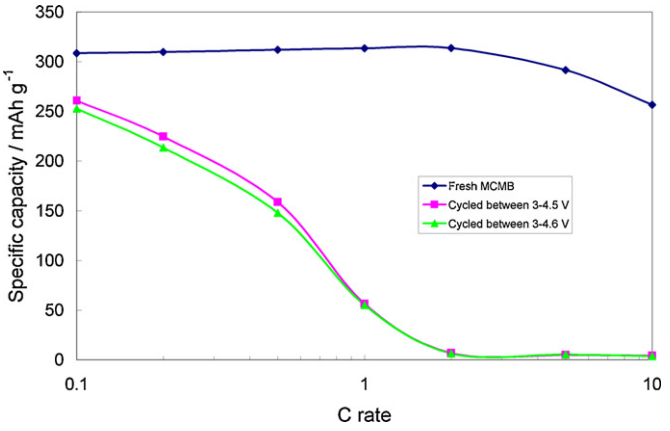

Fig. 12. Rate performances for the fresh and harvested MCMB anodes cycled against NCM cathode with 4.5 V and 4.6 V charge voltage limits.

performance of the MCMB-NCM full cells with different charge voltage limits. Fig. 3 shows a dramatic increase of dissolved metal ions in the electrolyte at potentials higher than 4.5 V. Considering the working potential of graphite anode is around 0.1 V, to avoid the severe dissolution of the metal ions into the electrolyte and the resultant effect on the anode, the upper voltage applied to the cell should not exceed 4.4 V. Based on the results seen of the full cycling, it is highly likely that the eventual capacity fade at 4.4 V is the result of the same mechanism as for the 4.5 V cell, except that the deposition and accumulation of transition metal cations on the anode surface were less obvious. Therefore, 4.3 V is determined to be the optimum charge voltage limit for the MCMB-NCM couple where both high energy density and excellent long term cycling behavior are achievable.

4. Conclusion

NCM cathode can be operated with very different charge voltage limits. The specific capacity and energy density is increased by elevation of the charge voltage limit. Meanwhile, dissolution of metal ions is dramatically increased at potentials higher than 4.5 V *vs.* Li/Li^+. In MCMB-NCM full cells, the dissolved metal elements found their way to the anode through separator *via* the electrolyte and deposited on the graphite surface, which induces a dramatic impedance rise of the negative electrode. Impedance rise is the most important reason responsible for the failure of the cell cycled with high charge voltage limit. Optimizing the charge voltage limit is an effective way to maintain low cell impedance and prolong the cycle life without sacrificing the energy output. The optimum charge voltage limit of 4.3 V is suggested for the MCMB-NCM lithium ion batteries having both high energy density and long cycle life.

Acknowledgements

This work was supported by the Assistant Secretary for Energy Efficiency and Renewable Energy, Office of Vehicle Technologies of the U.S. Department of Energy under Contract No. DE-AC02-05CH11231 and the Natural Science Foundation of China (NSFC 21073129).

References

[1] P. Albertus, J. Newman, J. Power Sources 183 (2008) 376–380.
[2] G. Liu, H. Zheng, A.S. Simens, A.M. Minor, V.S. Battaglia, J. Electrochem. Soc. 155 (2008) A887–A892.
[3] H. Huang, T. Faulkner, J. Barker, M.Y. Saidi, J. Power Sources 189 (2009) 748–751.
[4] A. Emori, A. Kudou, T. Horiba, Carbon 45 (14) (2007) 2857–2858.
[5] Y. Idemoto, T. Matsui, Solid State Ionics 179 (2008) 625–635.
[6] Y.W. Zeng, J. Power Sources 183 (2008) 316–324.
[7] K.A. Striebel, J. Shim, E.J. Cairns, R. Kostecki, Y.-J. Lee, J. Reimer, T.J. Richardson, P.N. Ross, X. Song, G.V. Zhuang, J. Electrochem. Soc. 151 (2004) A857–A866.
[8] S. Zhang, X. Qiu, Z. He, D. Weng, W. Zhu, J. Power Sources 153 (2006) 350–353.
[9] S.-K. Kim, W.-T. Jeong, H.-K. Lee, J. Shim, Int. J. Electrochem. Sci. 3 (2008) 1504–1511.
[10] G. Liu, H. Zheng, A.S. Simens, A.M. Minor, X. Song, V.S. Battaglia, J. Electrochem. Soc. 154 (2007) A1129–A1134.
[11] N. Yabuuchi, Y. Makimura, T. Ohzuku, J. Electrochem. Soc. 154 (2007) A314–A321.
[12] Y.J. Shin, W.-J. Choi, Y.-S. Hong, S. Yoon, K.S. Ryu, S.H. Chang, Solid State Ionics 177 (2006) 515–521.
[13] J. Park, J.H. Seo, G. Plett, W. Lu, A.M. Sastry, Electrochem. Solid State Lett. 14 (2) (2011) A14–A18.
[14] D.H. Jang, Y.J. Shin, S.M. Oh, J. Electrochem. Soc. 143 (1996) 2204–2211.
[15] Y. Xia, M. Yoshio, J. Electrochem. Soc. 143 (1996) 825–833.
[16] M. Wohlfahrt-Mehrens, C. Vogler, J. Garche, J. Power Sources 127 (1–2) (2004) 58–64.
[17] D. Aurbach, M.D. Levi, K. Gamulski, B. Markovsky, G. Salitra, E. Levi, U. Heider, L. Heider, J. Power Sources 82 (1999) 472–479.
[18] Y. Qin, Z. Chen, W. Lu, K. Amine, J. Power Sources 195 (2010) 6888–6892.
[19] Y. Zhang, C.-Y. Wang, J. Electrochem. Soc. 156 (2009) A527–A535.
[20] D.-C. Li, T. Muta, L.-Q. Zhang, M. Yoshio, H. Noguchi, J. Power Sources 132 (2004) 150–155.
[21] A. Deb, U. Bergmann, S.P. Cramer, E.J. Cairns, J. Appl. Phys. 97 (2005) 113523.
[22] J.J. Liu, W.H. Qiu, L.Y. Yu, G.H. Zhang, H.L. Zhao, T. Li, J. Power Sources 174 (2007) 701–704.
[23] P. Gao, G. Yang, H. Liu, L. Wang, H. Zhou, Solid State Ionics 207 (2012) 50–56.
[24] J. Li, Z.R. Zhang, X.J. Guo, Y. Yang, Solid State Ionics 177 (2006) 1509–1516.
[25] J.W. Fergus, J. Power Sources 195 (2010) 939–954.
[26] C. Huang, K. Huang, S. Liu, Y. Zeng, L. Chen, Electrochim. Acta 54 (2009) 4783–4788.
[27] Y. Liu, X. Li, H. Guo, Z. Wang, Q. Hu, W. Peng, Y. Yang, J. Power Sources 189 (2009) 721–725.
[28] J.S. Chen, L.F. Wang, B.J. Fang, S.Y. Lee, R.Z. Guo, J. Power Sources 157 (2006) 515–521.
[29] T. Aoshima, K. Okahara, C. Kiyohara, K. Shizuka, J. Power Sources 97 (2001) 377–380.
[30] L.-F. Wang, C.-C. Ou, K.A. Striebel, J.-S. Chen, J. Electrochem. Soc. 150 (2003) A905–A911.
[31] K. Xu, Chem. Rev. 104 (10) (2004) 4303–4418.
[32] T. Nakajima, M. Mori, V. Gupta, Y. Ohzawa, H. Iwata, Solid State Sci. 4 (2002) 1385–1394.
[33] D.P. Abraham, T. Spila, M.M. Furczon, E. Sammann, Electrochem. Solid State Lett. 11 (2008) A226–A228.
[34] Z. Chen, K. Amine, J. Electrochem. Soc. 153 (2006) A316–A320.